Low-complexity Digital Filter Geometry for Spherical Coded Imaging Systems

Guotong Feng[a], Mohammed Shoaib[b], and M. Dirk Robinson[a]

[a]Ricoh Innovations, Inc., 2882 Sand Hill Road Suite 115, Menlo Park, CA, USA;
[b]Department of Electrical Engineering, Princeton University, Princeton, NJ, USA

ABSTRACT

Recent research in the area of electro-optical system design identified the benefits of spherical aberration for extending the depth-of-field of electro-optical imaging systems. In such imaging systems, spherical aberration is deliberately introduced by the optical system lowering system modulation transfer function (MTF) and then subsequently corrected using digital processing. Previous research, however, requires complex digital post-processing algorithms severely limiting its applicability to only expensive systems. In this paper, we examine the ability of low-cost spatially invariant finite impulse response (FIR) digital filters to restore system MTF degraded by spherical aberration. We introduce an analytical model for choosing the minimum, and hence cheapest, FIR filter size capable of providing the critical level sharpening to render artifact-free images. We identify a robust quality criterion based on the post-processed MTF for developing this model. We demonstrate the reliability of the estimated model by showing simulated spherical coded imaging results. We also evaluate the hardware complexity of the FIR filters implemented for various spherical aberrations on a low-end Field-Programmable Gate Array (FPGA) platform.

Keywords: Electro-optical imaging, computational imaging, spherical aberration, spherical coding, Wiener filter, FIR filter, deblur, FPGA

1. INTRODUCTION

Spherical aberration (SA) is an image imperfection caused by the lens surface shape where the focus of incoming rays varies with the aperture. The effect of SA appears as blurs and low contrast in the captured image. In a traditional lens system, the spherical aberration effect is minimized by using combinations of concave and convex lenses or using aspheric lenses. Recent research in the area of electro-optical system design identified some potential benefits of spherical aberration for electro-optical imaging systems[1,2] These researches focused primarily on extending the depth-of-field using spherical aberration to achieve benefits similar to those of wave-front coding (CDM Optics).[3] In such imaging systems, which we call spherical coded imaging systems, spherical aberration is deliberately introduced by the optical system lowering system modulation transfer function (MTF) and then subsequently corrected using digital image processing. Imaging systems designed in this fashion provide a number of system-level advantages such as extended depth-of-field, better light collection ability, improved manufacturing tolerance, and lower component costs.[4] Previous researches in this area, however, require complex digital post-processing algorithms which severely limit its applicability to only expensive systems. We believe that these researches ignored key implementation issues necessary to make spherical coding practical for low-cost systems. Specifically, the previous research exploits computationally-expensive deconvolution techniques. The complexity of such digital processing algorithms precludes their use in real-time systems where computation resources are limited. We believe that the majority of real-time systems will instead rely on less expensive finite impulse response (FIR) filters.

Figure 1 shows a simulated example of spherical coded electro-optical imaging systems having three different spherical aberrations: 3 waves, 5 waves, and 7 waves. The left graph shows the optical MTFs for the three

Further author information: (Send correspondence to Guotong Feng)
Guotong Feng: E-mail: feng@rii.ricoh.com, Telephone: 1 650 496 5715

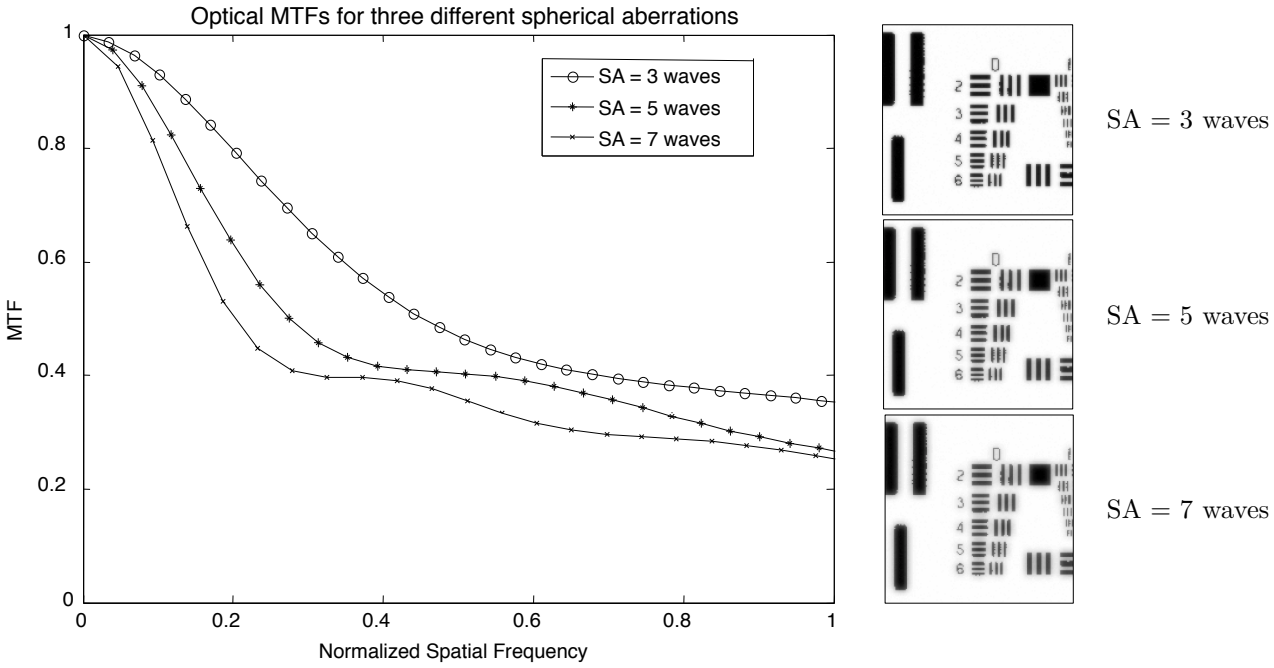

Figure 1. The diagram shows a simulated example of spherical coded imaging systems having three different spherical aberrations: 3 waves, 5 waves, and 7 waves. The left graph shows the optical MTFs for three spherical aberrations. The right graph shows the simulated images with various blurs due to different spherical aberrations. The variation of blurs in the images implies that an FIR filter with distinct frequency response is required for each spherical aberration to achieve high-quality imaging performance. Intuitively, larger blur with higher spherical aberration requires an FIR filter of larger geometry size for achieving desired sharpness.

spherical aberrations. Correspondingly, the right graph shows the captured images with various blurs due to different spherical aberrations. One identifiable characteristic of spherical coded systems is the low MTF values at low spatial frequencies. This corresponds to significant blurriness in the captured images which can be subsequently corrected with digital processing. Also, an important feature of spherical aberration is that the aberration is uniform over the field of view, and therefore independent of the radius location. This feature implies that a single spatially-invariant image sharpening filter may be sufficient to deblur the entire captured image. The significant variation of blurs in the images shown in Figure 1 implies that an FIR filter with distinct frequency response is required for each spherical aberration to achieve high-quality imaging performance. Intuitively, larger blur with higher spherical aberration requires an FIR filter with larger geometry size for achieving desired sharpness.

In this paper, we explore the relationship between optimal FIR filters characteristics and the magnitude of the spherical aberration in spherical coded systems. We introduce a simple analytical model for determining the minimum FIR filter size capable of providing the critical level sharpening to render artifact-free images. We apply a robust quality criterion based on the post-processed MTF for developing this model. We demonstrate the reliability of the estimated model by showing simulated spherical coded imaging results. We also evaluate the hardware complexity of the FIR filters designed for correcting various spherical aberrations.

The paper is organized as follows. In Section 2, we describe the FIR filter design for spherical coded imaging systems. In Section 3 we introduce a robust quality metric using MTF error function for identifying the relationship between the spherical aberration and the required FIR filter geometry. In Section 4, we present an analytical model characterizing the minimum FIR filter sizes for a broad class of spherical coded systems. Section 5 shows the hardware complexity of FIR filters as a function of the spherical aberration on a low-end Field-Programmable Gate Array (FPGA) platform. Finally, we make conclusions in Section 6.

2. DIGITAL FILTER DESIGN FOR SPHERICAL CODED SYSTEMS

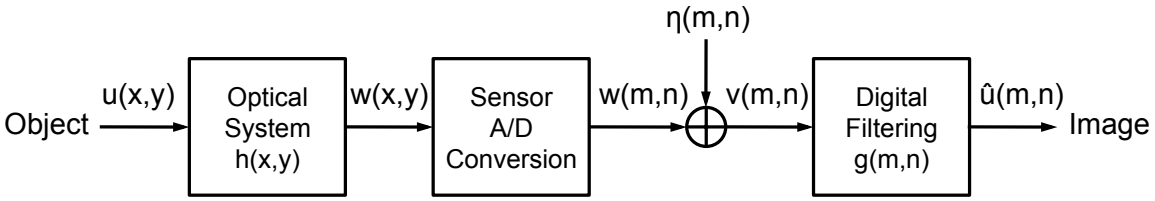

Figure 2. The diagram shows a simple image formation and restoration model of electro-optical imaging systems, which consists of a spatially invariant optical system, an image sensor with uniform sampling, and a digital filtering system for image restoration.

We describe the digital filter design procedure based on a simple image formation[5] and restoration model of electro-optical imaging systems. Figure 2 illustrates such a model which consists of a spatially invariant optical system, an image sensor with uniform sampling, and a digital filtering system for image restoration. For simplicity, we will be only focusing on the monochromatic imaging in this paper. Let $u(x, y)$ and $w(x, y)$ be the object signal input and the optical image output respectively. Let $h(x, y)$ be the point spread function (PSF) of the optical system. For spherical coded optical systems, we approximate the optical transfer function (OTF), which is the Fourier transform of the PSF, using the following equation:

$$H(\omega_1, \omega_2; W_{040}, W_{020}) = \mathcal{F}\left\{\left|\mathcal{F}\left\{M(\rho)\exp j2\pi(W_{040}\rho^4 - W_{020}\rho^2)\right\}\right|^2\right\} \ , \tag{1}$$

where $M(\rho)$ is a pupil amplitude function and ρ represents the pupil radial coordinates. Ideally, the spherical coded optical system will have a wavefront error function comprised of only two terms: a defocus term W_{020} and a spherical aberration term W_{040}. While this ignores the other aberrations found in real optical systems, we find that for reasonable field-of-view systems (FOV), the spherical aberration dominates the system performance of spherical coded systems.[4] We will use this form of the OTF approximation for designing and evaluating digital filters.

In the sensor A/D conversion process, the continuous signal space is converted to a discrete form, which leads to the Nyquist frequency limit. This means that for digital filter design, the OTF must be cropped out from the computed result in Equation 1 up to the Nyquist frequency. We define the undersampling factor U as the ratio of the Nyquist frequency of the detector system (defined by the pixel pitch size) over the diffraction-limited frequency of the optical system (depending on the f-number of the optical system).

$$U = \frac{\omega_N}{\omega_D} \ , \tag{2}$$

where ω_N is the Nyquist frequency defined by $\omega_N = 1/(2P)$, where P is the pitch size of each pixel, and ω_D is the diffraction-limited frequency defined by $\omega_D = 1/(\lambda F\#)$, where λ is the wavelength. Thus, the undersampling factor for a particular system is a function of the pixel pitch size and the f-number of the optical system. This undersampling factor is important in characterizing the digital-optical state of the imaging system. In this paper, we will focus on the imaging systems having undersampling factors in the range $U \in [0.05\ 0.30]$.

We apply the minimum mean square error (MMSE) criterion to our filter design process. In particular, we desire to obtain an estimated image, $\hat{u}(m, n)$, of the original (i.e. ideal digital) image $u(m, n)$ based on the sensor captured digital image $v(m, n)$ such that the mean square error

$$J = E\{(u(m, n) - \hat{u}(m, n))^2\} \tag{3}$$

is minimized.

2.1 Wiener filter design

If given unlimited computational resources, the ideal linear restoration filter (Wiener filter) for an electro-optical imaging system would have the spatial frequency response

$$G_{ideal}(\omega_1, \omega_2) = \frac{H^*(\omega_1, \omega_2)S_{uu}(\omega_1, \omega_2)}{|H(\omega_1, \omega_2)|^2 S_{uu}(\omega_1, \omega_2) + S_{\eta\eta}(\omega_1, \omega_2)} \ , \tag{4}$$

where G_{ideal} is the frequency response of the ideal Wiener filter, H is the monochromatic optical transfer function (OTF) given a fixed pair of W_{040} and W_{020}, S_{uu} is the power spectral density (PSD) of the original image signal, and $S_{\eta\eta}$ is the PSD of the noise added to the original image.[6] We assume that the additive noise PSD is flat with power σ_η^2 over the entire spectral frequency range. This ideal Wiener filter provides a balanced trade-off between contrast and signal-to-noise-ratio (SNR). We assume a commonly-used signal power spectral density model

$$S_{uu}(\omega_1, \omega_2) = \frac{d}{(1 + c_1^2 - 2c_1(1 - \omega_1^2))(1 + c_2^2 - 2c_2(1 - \omega_2^2))} \ , \tag{5}$$

where c_1 and c_2 are image correlation coefficients and d is a parameter which controls the signal power.[6] Here we choose d to achieve the unit signal power, i.e. $\sigma_u^2 = 1$. Achieving this ideal Wiener filter spectral response necessitates very large, if not infinitely large, FIR digital filters.

2.2 FIR filter design

To minimize the hardware costs, most digital processing systems use small FIR filters. Although the FIR filter is suboptimal compared to the infinite impulse response (IIR) filters in terms of filtering performance, it is more practical for real-time electro-optical imaging applications. Furthermore, FIR filters have no stability problems whereas IIR filters do have. In practice, optimal FIR filters can achieve performance approaching that of the IIR Wiener filters under certain conditions. In general, the larger the FIR filter sizes, the closer the FIR filter performance to that of the IIR Wiener filters. On the other hand, the computational cost (memory, speed, circuit area) is directly proportional to the size, shape, and the fixed-point coefficient precision of the digital FIR filter. In this paper, we will be only focusing on the FIR filter size by fixing the shape and the coefficient precision. The shape of an FIR filter is fixed to be $N \times N$ square, where N is the one-dimensional size of the filter. For the filter coefficient precision, we simply use the floating-point for our simulation.

Let g be the 1-D vector of the digital FIR filter coefficients containing N^2 elements, and $\hat{u}(m, n)$ be the filtered image processed by the FIR filter. Then the mean square error, J, of the FIR filtering process can be written as

$$J = \sigma_u^2 - 2g^T r_{uv} + g^T R_{vv} g \ , \tag{6}$$

where σ_u^2 is the signal power, R_{vv} an $N \times N$ block symmetric Toeplitz matrix of basic dimension $N \times N$ containing the known autocorrelation values of the captured image, and r_{uv} an $N^2 \times 1$ vector of the known cross-correlation values of the captured image and the ideal digital image.[6] To minimize the mean square error, the solution for Equation 6 can be written as the well-known Wiener-Hopf equation:

$$R_{vv} g = r_{uv} \ , \tag{7}$$

The Wiener-Hopf matrices are known to be positive definite and therefore non-singular yielding a unique solution to the determination of the Wiener filter coefficients. This solution, however, does not guarantee the unit DC power in the filtered images, which is important in digital image processing for electro-optical imaging systems. This means that there needs to be a unit energy constraint of the filter coefficients added to the minimization process for Equation 6, therefore the Wiener-Hopf solution may not be optimal under such constraint.

2.3 Normalized FIR filter design

The mean square error equation with the normalization constraint can be rewritten as

$$\begin{aligned} J = \frac{1}{2}\sigma_u^2 - g^T r_{uv} + \frac{1}{2} g^T R_{vv} g \\ \textit{subject to } Ag = 1 \ , \end{aligned} \tag{8}$$

where A is a vector of N^2 elements each having the value of 1. This equation leads to an equality constrained convex quadratic minimization problem, for which the solution can be expressed as

$$\begin{bmatrix} R_{vv} & A^T \\ A & 0 \end{bmatrix} \begin{bmatrix} g \\ q \end{bmatrix} = \begin{bmatrix} r_{uv} \\ 1 \end{bmatrix} \ , \tag{9}$$

where q is a scalar variable, and the coefficient matrix is called the KKT matrix.[7] It can be shown that the KKT matrix is nonsingular (see Appendix A), therefore there exists an unique optimal primal-dual pair (g^*, q^*) for Equation 9. We will use this solution for the optimal FIR filter design with various filter sizes in this paper.

Minimizing computational costs while achieving acceptable imaging performance is a goal of electro-optical imaging system. The key insight into FIR filter design for spherical coded systems is identification of the minimum FIR filter size which is capable of providing adequate image contrast (MTF) restoration. Intuitively, the size of the FIR filter should scale according to the size of the system's PSF. Traditional system designers do not typically encounter this question because the optical system is designed for maximum MTF contrast and hence have very small point spread functions. The typical image processing system uses very small digital filters having at most 5×5 filter taps. In contrast, spherical coded systems typically have much larger PSFs, and therefore require larger FIR filters.

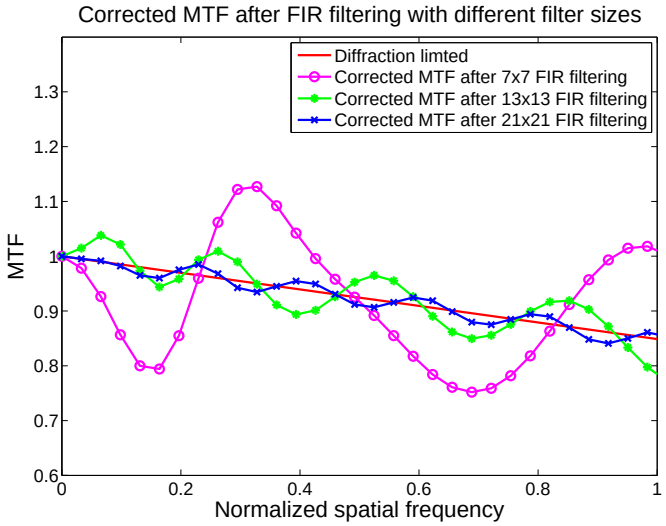

Figure 3. The diagram shows the corrected MTF after FIR filtering for three different filter sizes. The magenta curve shows the corrected MTF for the 7×7 FIR Wiener filter, the green curve for 13×13, and the blue curve for 21×21. All the three curves correspond to the spherical aberration of 7 waves and the undersampling factor of 0.12. All the three FIR filters are designed by choosing $c_1 = 0.85$, $c_2 = 0.85$, and $\sigma_\eta^2 = 1/100^2$ (*i.e.* $SNR = 40\ dB$).

Figure 3 shows the corrected MTF after FIR filtering for three different filter sizes. The corrected MTF is simply computed by multiplying the FIR filter frequency response with the optical MTF below the Nyquist frequency, which is written as

$$H_d(\omega_1, \omega_2) = H(\omega_1, \omega_2) G_{FIR}(\omega_1, \omega_2) \ , \tag{10}$$

where H_d is the corrected MTF, which we call digital-optical system MTF, and $G_{FIR}(\omega_1, \omega_2)$ is the frequency response of the FIR filter designed using Equation 9. The magenta curve shows the corrected MTF for the 7×7 FIR filter, the green curve for 13×13, and the blue curve for 21×21. All the three curves correspond to the spherical aberration of 7 waves and the undersampling factor of 0.12. All the three FIR filters are designed by choosing $c_1 = 0.85$, $c_2 = 0.85$, and $\sigma_\eta^2 = 1/100^2$ (*i.e.* $SNR = 40\ dB$). The 7×7 filter creates large magnitude of ripples in the corrected MTF especially at the lower frequency range, which implies that the performance of the filter in terms of MSE is poor. In comparison, the 13×13 filter creates much smaller ripples, and the 21×21 filter achieves the even better performance which is close to the ideal case. Overall, this diagram implies that an FIR filter size much larger than 5×5 is required for achieving good image filtering performance for systems with large spherical aberration.

3. QUALITY METRIC USING MTF ERROR FUNCTION

We introduce a robust quality metric for identifying the smallest FIR filter size capable of providing a critical level of MTF restoration. We define quality of MTF restoration as a weighted departure from an ideal MTF

function which we call the MTF error function. The MTF error function is computed as

$$E_{mtf} = \int_0^1 \int_0^1 |T(\omega_1, \omega_2) - H_d(\omega_1, \omega_2)|^2 \, S_{uu}(\omega_1, \omega_2) d\omega_1 d\omega_2 \ , \tag{11}$$

where the MTF error function E_{mtf} is a weighted departure of the corrected MTF, $H_d(\omega_1, \omega_2)$, from an ideal MTF function denoted by $T(\omega_1, \omega_2)$, and $S_{uu}(\omega_1, \omega_2)$ plays the role of a weighting function.

Figure 4 shows an example of the MTF error function for two different optical systems as a function of the filter size N for $N \times N$ FIR filters. The blue curve shows the MTF error for a high-quality, nearly aberration-free optical system. In this case, the MTF error is negligible due to high-quality optics. The red curve shows the MTF error for a spherical coded system. In this case, the MTF error drops precipitously until about $N = 9$ after which the MTF error becomes negligible. This demonstrates the key relationship between the minimum filter size and the ability to restore spherical coded systems. Through experimentation, we have identified 0.2

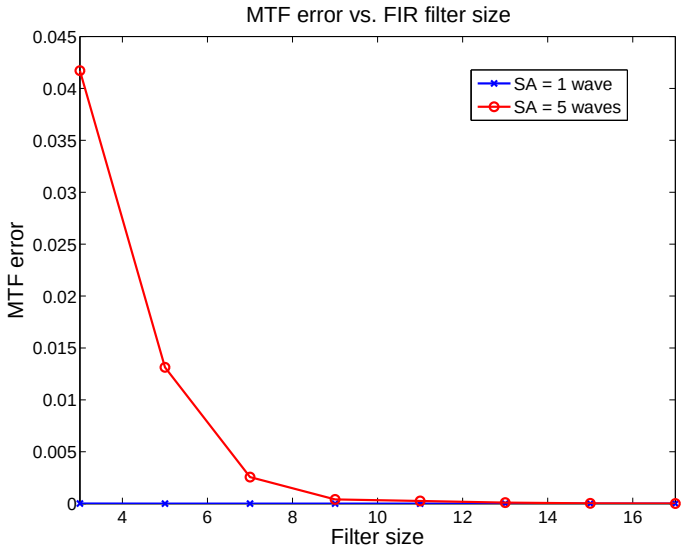

Figure 4. The diagram shows the MTF error as a function of filter size N for $N \times N$ FIR filters . The red curve shows the MTF error for spherical aberration of 5 waves, and the blue curve shows the MTF error for spherical aberration of 1 wave. Both curves have the same undersampling factor of 0.12. The traditional system which has a small PSF requires only minimal filtering. The spherical coded system, however, requires at least a 9×9 to achieve acceptable MTF restoration.

percent MTF error as being nearly indistinguishable from the ideal Wiener filter, and also producing minimal visual errors.

Figure 5(a) shows an example of a simulated image captured by a spherical coded imaging system having spherical aberration of 5 waves and undersampling factor of 0.12. The spherical coding produces the telltale halos around the objects. Figures 5(b)-(f) show the resulting images after being sharpened by 3×3, 5×5, 7×7, and 9×9 tap filters and the image produced when sharpened by the ideal Wiener filter. The smaller filters are unable to correct the halo artifacts due to their small sizes (see the electronic version of this paper for more details of the images). The 9×9 filter achieves nearly the same performance as the ideal Wiener filter.

4. OPTIMAL FILTER SIZES FOR SPHERICAL CODED SYSTEMS

As we have shown, for spherical coded systems to provide high-quality images, the digital filters require a certain size. This minimal size is a function of both the strength of the spherical coding as well as the undersampling factor U at which the system is operating. The ideal digital filters should be large enough to restore contrast but not large enough to increase the complexity of the digital processing system. In this section, we identify

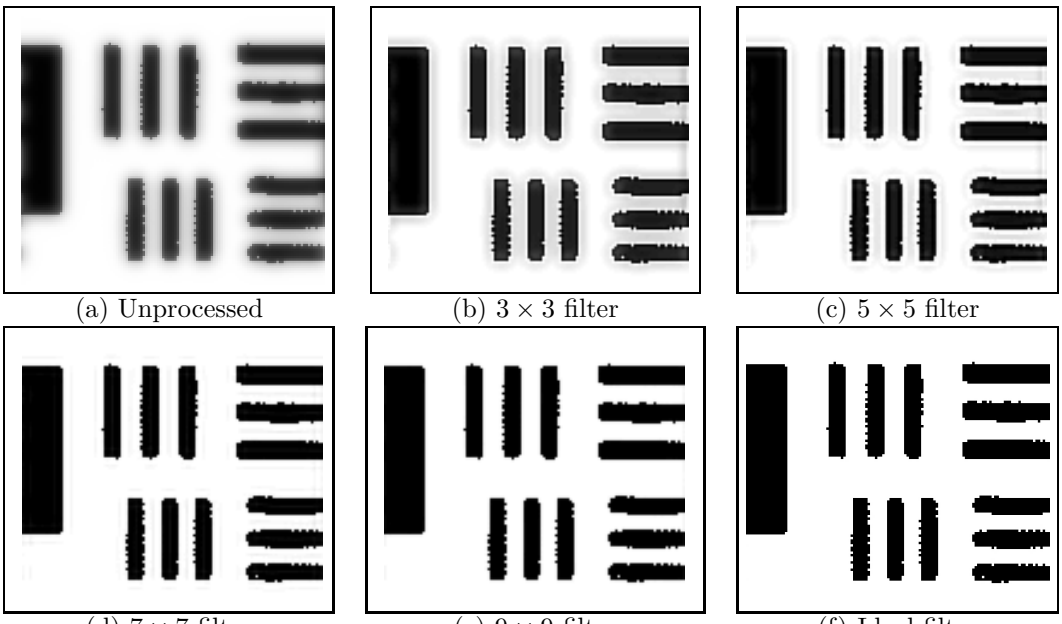

(a) Unprocessed (b) 3×3 filter (c) 5×5 filter

(d) 7×7 filter (e) 9×9 filter (f) Ideal filter

Figure 5. The image in (a) shows a simulated image captured by a spherical coded optical system having spherical aberration of 5 waves and undersampling factor of 0.12. The image exhibits the halo artifacts around the objects. Images (b)-(f) show the results after being sharpened by a 3×3, 5×5, 7×7, 9×9, and ideal Wiener filter. The 3×3, 5×5, and 7×7 filters are too small to remove the halos (see the electronic version of this paper for more details of the images). The 9×9 filter produces an image nearly indistinguishable from the ideally-filtered image.

the minimum filter size required to achieve acceptable system-level performance for a range of spherical coded imaging systems.

We have identified a space of optical systems which we believe will benefit from spherical coding. We examine spherical aberration in the range $W_{040} \in [0, 8]$ waves and under-sampling factor in the range $U \in [0.05\ 0.30]$. Undersampling factors outside of this range correspond to either extremely low-resolution systems, or extremely high-resolution system (e.g. microscopes). For every pair (W_{040}, U), we identify the minimum filter size required to achieve at least 0.2 percent MTF error.

To ensure that we are truly finding the minimum filter size, we vary the defocus of the systems (W_{020}) so as to minimize the MSE of the system. The system MSE is defined as follows

$$\begin{aligned} E_{mse}(W_{020}) &= \int_0^1 \int_0^1 |T(\omega_1, \omega_2) - G_{ideal} H(\omega_1, \omega_2; W_{040}, W_{020})|^2 S_{uu}(\omega_1, \omega_2) \\ &\quad + \sigma_\eta^2 |G_{ideal}(\omega_1, \omega_2)|^2 d\omega_1 d\omega_2 \ , \end{aligned} \tag{12}$$

where W_{040} is fixed, and W_{020} is variable. There exist other criteria for determining the best defocus for an optical system.[8] We choose MSE to determine the best defocus because it is a good criterion for the end-to-end electro-optical system performance measure[9].[4]

Figure 6 shows an example of how the MSE performance changes with the system defocus. The MSE for each defocus position is computed for the ideal Wiener filter designed using Equation 4 with the spherical aberration $W_{040} = 7\ waves$, $c_1 = 0.85$, $c_2 = 0.85$, and $\sigma_\eta^2 = 1/100^2$. In this example, the best defocus for the minimal MSE performance is found at $W_{020} = 2$. We then apply this defocus value to compute the MTF for the subsequent FIR filter analysis for all different sizes.

The left image of Figure 7 shows the experimentally obtained minimum filter sizes $N \times N$ required to achieve acceptable image restoration for a space of electro-optical imaging systems with $W_{040} \in [0, 8]$ waves and $U \in [0.05, 0.3]$. The lower left corner of the image corresponds to low-resolution systems with minimal aberration.

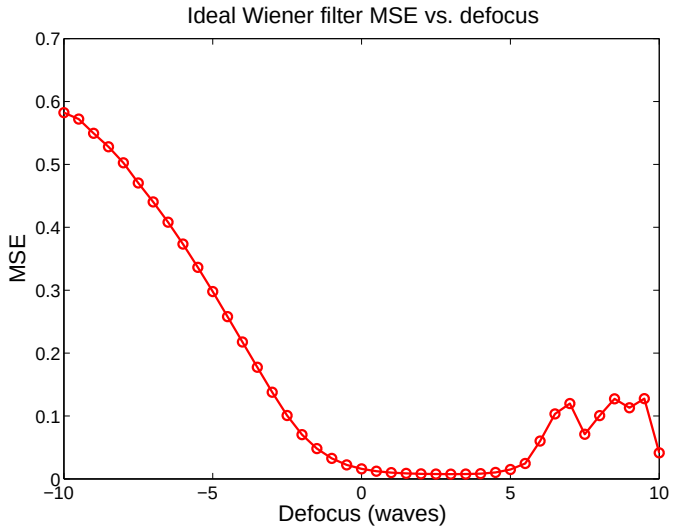

Figure 6. The diagram shows an example of how the MSE performance changes with the system defocus. The MSE for each defocus position is computed for the ideal Wiener filter designed using Equation 4 with the spherical aberration $W_{040} = 7$ *waves*, $c_1 = 0.85$, $c_2 = 0.85$, and $\sigma_\eta^2 = 1/100^2$. In this example, the best defocus for the minimal MSE performance is found at $W_{020} = 2$.

This corresponds to the traditional, uncoded optical systems. As such, the systems require only small FIR filters. As we move up towards the top of the image, the strength of the spherical coding increases, thereby requiring larger digital filters. Likewise, as we move to the right, the resolution of the optical systems increases, thereby effectively increasing the perceived effect of the spherical aberration, and hence also requiring larger filters.

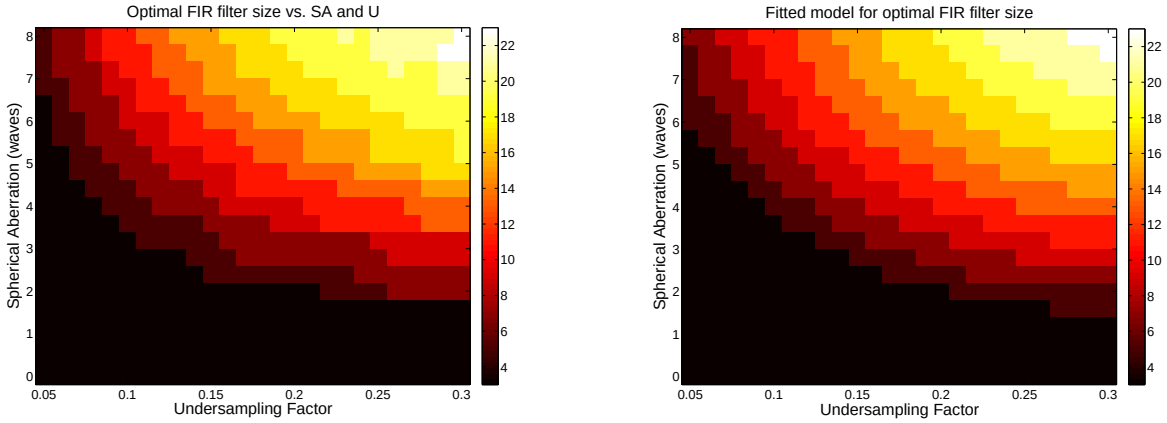

Figure 7. The left image shows the minimal FIR filter sizes required for the spherical coded system in the parameter space of the spherical aberration ($W_{040} \in [0, 8]$ waves) and the undersampling factor ($U \in [0.05, 0.3]$). The right image shows a fitted model using a second-order polynomial fitting function.

The minimum required filter sizes show very regular behavior as a function of spherical aberration strength and the undersampling factor. By fitting a second-order polynomial function to the experimentally-obtained data, we are able to analytically describe the relationship between the optimal filter size and the type of spherical coded system. The image on the right side of Figure 7 shows the result of this second-order polynomial approximation. Each of the filter sizes satisfies the required quality criterion of at least 0.2 percent MTF error. The required filter size is $N \times N$, where N is defined in the following:

a_1	a_2	a_3	b_1	b_2	c
-0.191	-150.0	4.12	3.52	86.7	-15.3

Table 1. The parameters of the estimated model of optimal FIR filter sizes for spherical coded systems with $W_{040} \in [0, 8]$ waves and $U \in [0.05, 0.3]$.

$$N = max(3, N_f) , \tag{13}$$

where N_f is a quadratic function of W_{040} and U expressed as

$$N_f = a_1 W_{040}^2 + a_2 U^2 + a_3 W_{040} U + b_1 W_{040} + b_2 U + c , \tag{14}$$

where the values of the coefficients a_1, a_2, a_3, b_1, b_2, and c are listed in Table 1.

This estimated model enables the system designers to quickly adjust high-level optical design parameters and predict digital system costs using only two simple digital-optical characteristics, spherical aberration in wavelengths, and the ratio of the diffraction-limited Airy spot size over the pixel pitch.

5. HARDWARE COMPLEXITY

In this section, we briefly demonstrate the hardware implementation and complexity of the FIR filters for various spherical aberrations on a low-end FPGA platform, Xilinx Spartan-3E . Figure 8 shows the direct form FIR filter architecture using Multiply-Accumulate (MAC),[10] which is commonly used in hardware implementation. As shown in the figure, $c_i, i = 0, 1, ...L-1$, represents the constant filter coefficient for each tap, where L is the total number of filter taps, which, in our case, is N^2. The value of each coefficient is pre-determined by converting the floating-point coefficient of the optimally designed FIR filter to a fixed-point value. In our implementation, we use 12 bits to represent the fixed-point coefficient values. We found that this bit precision is just high enough to achieve the desired MTF error for all targeted spherical coded systems.

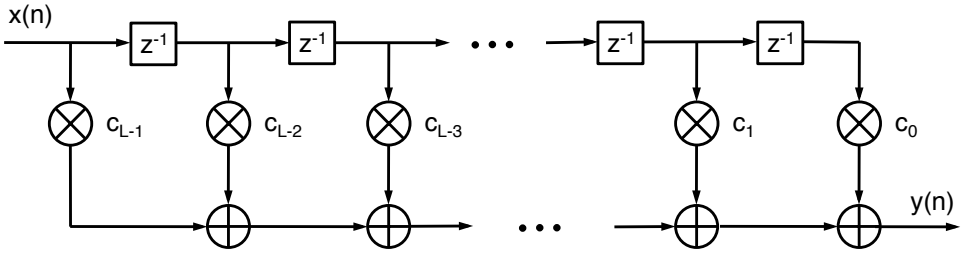

Figure 8. This diagram shows the direct form FIR filter architecture using Multiply-Accumulate (MAC). $c_i, i = 0, 1, ...L-1$, represents the constant filter coefficient for each tap, where L is the total number of filter taps.

Figure 9 and Table 2 show the circuit area (slice and 4-Input Look-Up-Table (LUT) numbers) utilized by the FIR MAC on the Xilinx Spartan-3E FPGA as a function of the spherical aberration ranging from 2 to 8 wavelengths at the undersampling factor 0.20. Observe that the FPGA area increases approximately linearly as the spherical aberration increases. Note that the curve decreases by a certain number at some points because the FPGA implementation complexity also depends on the specific filter coefficient values other than the filter sizes.

6. CONCLUSIONS

We introduced a class of electro-optical spherical coded imaging systems that achieve high-quality imaging performance using low-complexity digital FIR sharpening filters. Such imaging systems have a number of system-level advantages such as extended depth of field, better light collection ability, and improved manufacturing yield.

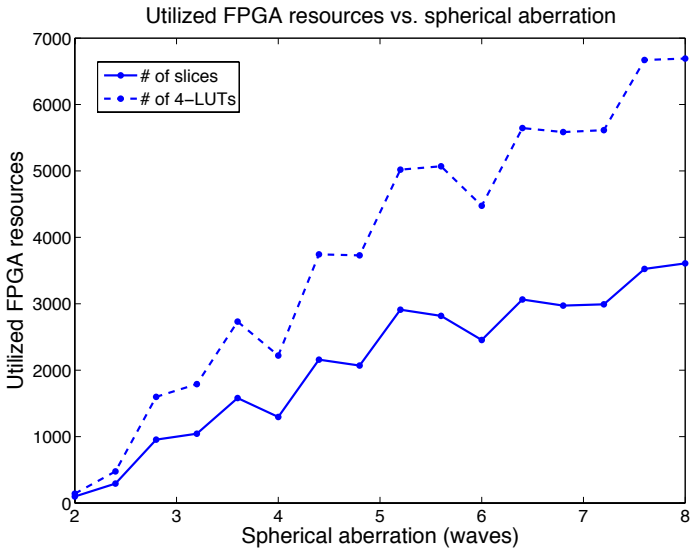

Figure 9. This diagram shows the circuit area (slice and 4-Input LUT numbers) utilized by the FIR MAC filter in the Xilinx Spartan-3E FPGA as a function of the spherical aberration ranging from 2 to 8 wavelengths at the undersampling factor 0.20.

Filter Size	SA (waves)	#(%) Slices	#(%) 4-LUTs	#(%) MULT18x18SIO
3x3	2.0	98 (2)	141 (1)	9 (45)
5x5	2.4	293 (6)	476 (5)	20 (100)
7x7	2.8	954 (20)	1598 (17)	20 (100)
7x7	3.2	1044 (22)	1790 (19)	20 (100)
9x9	3.6	1581 (33)	2731 (29)	20 (100)
9x9	4.0	1295 (27)	2220 (23)	20 (100)
11x11	4.4	2158 (46)	3744 (40)	20 (100)
13x13	4.8	2069 (44)	3729 (40)	20 (100)
13x13	5.2	2911 (62)	5019 (53)	20 (100)
13x13	5.6	2818 (60)	5070 (54)	20 (100)
15x15	6.0	2454 (52)	4476 (48)	20 (100)
17x17	6.4	3064 (65)	5646 (60)	20 (100)
17x17	6.8	2973 (63)	5585 (59)	20 (100)
17x17	7.2	2992 (64)	5614 (60)	20 (100)
19x19	7.6	3524 (75)	6670 (71)	20 (100)
19x19	8.0	3608 (77)	6692 (71)	20 (100)

Table 2. Utilization of FPGA resources of the FIR filters required for various amounts of spherical aberration. SA is the spherical aberration in wavelengths. " #" indicates the utilized resource number, and "%" the percentage of the utilized resource over the total number of that resource in the FPGA. MULT18x18SIO indicates embedded multipliers in the FPGA.

We analyzed the ability of spatially invariant FIR digital filters for compensating various amounts of spherical aberration, and provided an analytical model to determine minimum FIR filter sizes that are required for the entire class of spherical coded systems. We also identified a reliable quality criterion used for developing this model. Finally, we evaluated the relationship between hardware complexity and spherical aberration on a low-end FPGA platform.

APPENDIX A. PROOF OF THE NONSINGULARITY OF THE KKT MATRIX

Based on the blockwise matrix inversion theory, the inverse of the KKT matrix $\begin{bmatrix} R_{vv} & A^T \\ A & 0 \end{bmatrix}$ is equivalent to $\begin{bmatrix} R_{vv}^{-1} + R_{vv}^{-1}A^TB^{-1}AR_{vv}^{-1} & -R_{vv}^{-1}A^TB^{-1} \\ -B^{-1}AR_{vv}^{-1} & B^{-1} \end{bmatrix}$, where $B = -AR_{vv}^{-1}A^T$. Note that B is a scalar. Since R_{vv}^{-1} exists, we only need to show that B^{-1} exists. It has been shown that the inverse of a positive definite matrix is also positive definite, therefore R_{vv} being positive definite leads to $B < 0$ for $A = [1, 1, ...1]$. Hence the inverse of the KKT matrix exists.

REFERENCES

[1] Mouroulis, P., "Depth of field extension with spherical optics," *Optics Express* **16**(17), 12995–13004 (2008).

[2] George, N. and Chi, W., "Extended depth of field using a multi-focal length lens with a controlled range of spherical aberration and a centrally obscured aperture," *USPTO Patent* (7336430) (2008).

[3] Dowski, E. and Cathey, W. T., "Extended depth of field through wave-front coding," *Applied Optics* **41**(11), 1859–1866 (1995).

[4] Robinson, M. D., Feng, G., and Stork, D. G., "Spherical coded imagers: Improving lens speed, depth-of-field, and manufacturing yield through enhanced spherical aberration and compensating image processing," *Proceedings of SPIE Optics + Photonics Conference* (August 2009).

[5] Maeda, P., Catrysse, P. B., and Wandell, B. A., "Integrating lens design with digital camera simulation," *Proceedings of SPIE Electronic Imaging* **5678**, 48–58 (February 2005).

[6] Jain, A. K., [*Fundamentals of Digital Image Processing*], Prentice Hall, Englewood Cliffs, New Jersey, first ed. (1989).

[7] Boyd, S. and Vandenberghe, L., [*Convex Optimization*], Cambridge University Press, Cambridge, UK, first ed. (2004).

[8] Smith, W. J., [*Modern Optical Engineering*], McGraw-Hill, New York, NY (2000).

[9] Stork, D. G. and Robinson, M. D., "Theoretical foundations for joint digital-optical analysis of electro-optical imaging systems," *Applied Optics* **47**(10), B64–B75 (2008).

[10] Meyer-Baese, U., [*Digital Signal Processing with Field Programmable Gate Arrays*], Springer-Verlag, New York, NY, third ed. (2007).